Excretable, ultrasmall hexagonal NaGdF4:Yb50% Nanoparticles for bimodal imaging and radiosensitization

Jossana Abcede Damasco
University of Texas MD Anderson Cancer Center
Tymish Y Ohulchanskyy
University at Buffalo - The State University of New York
Supriya D Mahajan
University at Buffalo - The State University of New York
Guanying Chen
University at Buffalo - The State University of New York
Ajay Singh
University at Buffalo - The State University of New York
Hilliard Kutscher
University at Buffalo - The State University of New York
Haoyuan Huang
University at Buffalo - The State University of New York
Steven Turowski
Roswell Park Comprehensive Cancer Center
Joseph A Spernyak
Roswell Park Comprehensive Cancer Center
Anurag Singh
Roswell Park Comprehensive Cancer Center
Jonathan F Lovell
University at Buffalo - The State University of New York
Mukund Seshadri
Roswell Park Comprehensive Cancer Center
Paras Prasad (pnprasad@buffalo.edu)
University at Buffalo - The State University of New York

Research

Keywords: gadolinium nanoparticles, radiosensitizer, theranostics, MR/CT imaging probes, glioblastoma

Posted Date: September 4th, 2020

DOI: https://doi.org/10.21203/rs.3.rs-61672/v1

Version of Record: A version of this preprint was published on February 5th, 2021. See the published version at https://doi.org/10.1186/s12645-021-00075-x.

Abstract

Background

In this study, we report on the synthesis, imaging properties and radiosensitizing properties of β-$NaGdF_4$:Yb50% nanoparticles as a multifunctional theranostic platform. The synthesized nanoparticles act as potent bimodal contrast agents with superior imaging properties compared to existing agents used for magnetic resonance imaging (MRI) and computed tomography (CT). Clonogenic assays demonstrated that these nanoparticles can act as effective radiosensitizers, provided the nanoparticles are taken up intracellularly.

Results

A 2 Gy dose of X-ray induced ~ 20% decrease in colony survival when C6 rat glial cells were incubated with non-targeted nanoparticles ($NaGdF_4$:Yb50%), whereas the same X-ray dose resulted in a ~ 60% decrease in colony survival with targeted nanoparticles conjugated to folic acid ($NaGdF_4$:Yb50%-FA). Intravenous administration of nanoparticles resulted in clearance through urine and feces within a short duration, based on the *ex vivo* analysis of Gd^{3+} ions *via* ICP-MS.

Conclusion

These biocompatible and in vivo clearable ultra-small $NaGdF_4$:Yb50% are promising candidates for further evaluation in image-guided radiotherapy applications.

Background

Clinically relevant, multifunctional nanoparticles that combine diagnostic and therapeutic platforms are of high scientific interest, with significant societal impact. [1–3] However, these theranostic nanomaterials often result in complex and large-sized structures in order to accommodate the various components that provide multi-functionality. In addition, complicated synthesis methods are difficult to reproduce and can be impractical for large-scale processing.

In order to be clinically relevant, nanomaterials need to exhibit biocompatibility and ideally undergo rapid clearance from the body. [4] Nanoparticles are primarily taken up and eventually cleared by the reticuloendothelial system (RES) or kidneys. However, retention in the liver or spleen can take up a long time depending on their size and surface chemistry. [5, 6] In general, large non-degradable nanoparticles with hydrodynamic size > 8 nm are not easily cleared from the body within a reasonable time period. [7, 8] A pilot study in nonhuman primates of CdSe/CdS/ZnS quantum dots (QDs) (7–8 nm) showed 90% of the initial dose was retained in the liver, spleen, and kidneys, 90 days following intravenous (IV) injection, with no evidence of toxicity. [9] Amphiphilic polymer coated CdSe/ZnS QDs (10–30 nm) were confined to

sentinel lymph nodes of mice for at least 2 years, although they exhibited minimal toxicity as assessed by pathological examination. [10] These accumulations in the RES and the slow elimination, taking months or even years to clear the body, can be problematic for clinical translation. On the other hand, clearance through the kidneys occurs quickly, as the nanoparticles are filtered from the blood and excreted out. This significantly reduces the risk of potential toxicity, which makes the renal clearance pathway an attractive route of elimination. [11] However, glomerular filtration is strongly dependent on size, with a hydrodynamic diameter filtration-size threshold of < 6 nm. [7] Thus, the development of ultrasmall, biocompatible, multifunctional nanoparticles is of high interest for potential clinical use.[7, 12, 13]

One of the promising applications of theranostic nanoparticles is their ability to enhance radiotherapeutic efficacy. Radiation therapy (RT) is an integral part of the clinical management of most solid tumors, and remains one of the most cost-effective treatments for cancer patients.[14] However, not all patients respond to RT, and disease recurrence remains a significant clinical problem.[15]

The use of nanoparticles to ‘sensitize’ tumors to RT could potentially enable lowering of the total radiation dose administered to patients without compromising efficacy. Furthermore, radiation-induced normal tissue toxicity often contributes to a poor quality of life (QOL) in patients. Optimal use of these nanoparticles in combination with RT may therefore minimize collateral radiation damage to normal tissues and potentially improve QOL.

In this regard, there is growing interest in the use of metal nanoparticles containing high Z-elements as radiosensitizers. Upon interaction with X-rays, nanoparticles with high atomic number are known to enhance the photoelectric and Compton effects, increasing the emitted secondary electrons resulting in radiation dose-enhancements.[14] Most studies have focused on gold (Z = 79) nanoparticles and significant evidences have been reported to demonstrate their ability to increase the therapeutic ratio of radiotherapy. [16–19] Hafnium oxide (Z = 72) developed by NanoBiotix (France), has already shown success in the clinic as efficient radiation enhancers on patients requiring preoperative radiotherapy.[20] Other metal nanoparticles that have shown great promise in augmenting radiotherapy include bismuth (Z = 83) [21]; platinum (Z = 78) [22, 23] and iron oxide[24, 25] having both radiosensitizing and hyperthermic [26] properties.

Both gadolinium-based (Z = 64) and ytterbium-based (Z = 70) nanoparticles have garnered attention as theranostic platforms. Gd-based nanoparticles have been shown to enhance magnetic resonance (MR) imaging contrast and have been found to induce X-ray dose enhancement, making them ideal candidates for combined imaging and therapy, and are currently in Phase I clinical trial for the treatment of multiple brain metastases.[27–29] Yb-based nanoparticles have been developed as bimodal probes for X-Ray computed tomography (CT) and near infrared-to-near infrared fluorescence imaging. [30] The high X-ray attenuation of Yb enabled its use as a theranostic agent, with both tumor imaging and radiosensitization functions. [31]

In this study, we present nanoparticles containing Gd and Yb as candidates for combined imaging and therapy in a single ultra-small nanoplatform for cancer therapy. The combination of Gd and Yb allows for the nanocrystal serving as a bimodal imaging probe for MR and CT examinations. MR imaging is best suited for soft tissue imaging while X-ray CT is ideal for hard tissues or bone. The first reported use of combined Gd and Yb as an MR/CT probe was in the form of $NaGdF_4$:Yb20% doped with 2% Erbium(Er) for additional optical imaging capability. [32] In addition, CT signal was enhanced by increasing the amount of Yb from 20–80% (i.e., $NaYbF_4$:Gd20%). [33] Therefore our nanoparticles were designed with an equimolar amount of Gd^{3+} and Yb^{3+} ions to maximize both properties. In addition, reducing the size of the nanoparticles to sub-5 nm increases the surface Gd^{3+} accessible to H_2O which leads to higher T1 relaxivities in comparison to larger nanoparticles,[34] while allowing complete elimination from the body within days (i.e., 4 days) through hepatic and renal clearance, as revealed from our ICP-MS analysis of Gd^{3+}. To ensure effective radiosensitization, these nanoparticles were modified for targeted delivery by conjugating folic acid to their surface, ensuring optimal cellular uptake by cancer cells, which ultimately significantly decreased the number of surviving colonies following a clinically relevant X-ray exposure. Ultrasmall size is also ideal for radiotherapy as the effective secondary electrons are generated only by the surface and a few layers within, resulting in localized DNA damage.

We evaluated the efficacy of this nanoplatform in an *in vitro* clonogenic assay using C6 rat glioblastoma cells. Glioblastoma multiforme (GBM) is the most aggressive form of gliomas with a median survival of ~ 12 months in patients.[35] A major factor that contributes to poor prognosis in GBM patients is the limited response to treatment caused by the inability of most chemotherapeutic agents to cross the blood-brain barrier (BBB). We demonstrate here that the ultrasmall size of the nanoparticles conjugated with folic acid can take advantage of the folate receptor expressed at the BBB [36, 37] to facilitate the transport of the nanoparticles. Given the marked signal enhancement on both MR and CT imaging, our nanoparticles could enable accurate diagnosis of disease progression of GBM.

With its facile synthesis, highly uniform size distribution, ultrasmall size and easily tailored surface, these novel nanoparticles present a promising, translatable theranostic platform with high tumor uptake, favorable biodistribution and route of elimination.

Results

Formation of Ultrasmall β-$NaGdF_4$:Yb50%

Uniform sub-5 nm $NaGdF_4$:Yb50% nanoparticles in a thermodynamically stable, hexagonal phase (β-phase) were successfully synthesized. Analysis of more than 100 nanoparticles from TEM images reveals a normal size distribution with an average diameter of 3.44 nm ± 0.72 nm (Figure 1a-c). The formation of ultrasmall β-$NaGdF_4$:Yb50% nanoparticles is confirmed by its very broad X-ray diffraction patterns, which conform to the standard XRD peaks of the hexagonal β-phase $NaGdF_4$ (JCPDS 27-0699) (Figure 1d). Elemental analysis of Gd and Yb content shows the respective actual molar percentages to

be 52.18% and 47.82%, a clear indication that the desired stoichiometric amount of Yb^{3+} ions were successfully doped into the $NaGdF_4$ nanoparticle.

Surface modification of the nanoparticle surface was achieved through ligand exchange by allowing the nanoparticles in chloroform solution, and the L-cysteine and DTPA anhydride in basic water (pH 9) to mix for 24 h. The hydrodynamic diameter measured by dynamic light scattering (DLS) showed an increase in the hydration shell from 4.1 nm (in hexane) to 5.1 nm (in H_2O) (Figure S3) after surface modification. TEM images did not show clustering or aggregation of the nanoparticles suspended in H_2O (Figure S4). This successful coating of the ligands on the nanoparticle surface also provided additional functional groups (i.e., amine and carboxylate) to allow bioconjugation of targeting ligands.

Gd^{3+}Leaching, Cytotoxicity and Biodistribution

Stability of $NaGdF_4$ was evaluated by measuring the Gd^{3+} ion leakage from the crystal matrix. Analysis of Gd^{3+} leaching show less than 0.1% Gd^{3+} ions were present when dialyzed against H_2O. Solutions of DMEM with 10% FBS, and DMEM with 10% FBS supplemented with 10 mM phosphate, incubated at 37^0C, were utilized to mimic physiological conditions and to assess the effect of elevated phosphate levels on the stability of the nanoparticles. After 3 days of dialysis, ~2% of the Gd^{3+} was observed in dialysate; this rose to ~3% at higher phosphate concentrations (Figure 3a).

The effect of the nanoparticles on cell viability was studied by monitoring the mitochondrial metabolic activity through the standard MTS assay. C6 cells remained 100% viable after 12 and 24h incubation at up to 1 mg/mL (Figure 3b). More importantly, cells remained 100% viable even with increased incubation time (48h), at 125 µg/mL. It is generally accepted that nanoparticle toxicity is concentration- and time-dependent.[38, 39] Similarly, further increase in the concentration of the nanoparticles to 1 mg/mL at prolonged exposure time (i.e., 48 h) resulted in increased cytotoxicity (50% of cell viability).

Passive biodistribution and clearance study revealed that less than 0.5% of the nanoparticles remained in the organs after 4 days, as detected by ICP-MS (Figure 3c). After 4 h, 33% of the nanoparticles were eliminated in the urine and 21% in the feces (Figure 3d). The remaining nanoparticles were eliminated mostly in the feces over the period of 4 days (Figure 3d).

Nanoparticles for MRI and CT Imaging

The potential of these nanoparticles as a bimodal imaging probe for both MR and CT imaging was evaluated by measuring their T1 relaxivity (*r1*) and the Hounsfield unit (HU) values, respectively. The relaxivity of the nanoparticles was compared to Gd-DTPA (Magnevist®) at 25°C and 37°C by measuring T1 rates of a series of solutions containing increasing Gd^{3+} molar concentrations (as determined by ICP-OES). There is a linear relationship between the Gd^{3+} concentration and the longitudinal relaxation rate (1/T1), and *r1* values are determined from the slope of the resulting linear plots (Figure S5). A pseudo-colorized, T1-weighted spin echo image (TE/TR = 8.5/500ms) for saline, 200 µM Gd-DTPA and

nanoparticles (200 μM [Gd]) demonstrates the improvement in T1-weighted contrast of the nanoparticles over the standard clinical MR imaging agent Gd-DTPA (Figure 4b).

The Hounsfield unit (HU) value, determined from the slope of the linear plot of HU as a function of the concentration, can indicate if the nanoparticles can serve as a CT contrast agent. There is a linear correlation between the increasing contrast agent concentration and the CT signal intensity for both the commercial agent iohexol and the nanoparticle solution (Figures 5a and 5c). The nanoparticles and iohexol show almost identical line slopes (Figures 5b and 5d) indicating similar signal enhancement capabilities. Setting the HU value of water as zero, the calculated HU value for the ultrasmall $NaGdF_4$:Yb50% is approximately 26 HU while that of the iohexol is about 23 HU.

Nanoparticles as a Radiosensitizer

A clonogenic assay was used to investigate the potential of the nanoparticles as radiosensitizers in a rat C6 glioma cell line. To ensure that cell death was not due to the inherent toxicity of the nanoparticles, the concentration was kept at 100 μg/mL, which still maintained more than 90% cell viability even after 48h incubation (Figure 3b). Colony formation of the cells without nanoparticles and without X-ray radiation treatment served as control. C6 cells incubated with nanoparticles but not subjected to X-ray radiation did not reduce surviving colonies confirming that the nanoparticle concentration was not cytotoxic (Figure 6). Irradiation alone of the cells with a 2 Gy dose did not result in any significant cell reproductive death. Cells treated with non-targeted $NaGdF_4$:Yb50% nanoparticles showed a 16% decrease in surviving colonies, in comparison to cells treated only with X-ray radiation. In comparison, targeted $NaGdF_4$:Yb50%-FA nanoparticles demonstrated superior efficacy with only 40% surviving colonies when treated with 2 Gy radiation.

Nanoparticles cross the Blood-Brain-Barrier

To further test the potential application of these ultrasmall nanoparticles to treat brain tumors, the ability to cross the blood-brain barrier (BBB) was explored utilizing a previously reported cell-based two-chamber *in vitro* transwell model of the BBB.[40, 41]. Both non-targeted and FA-targeted nanoparticles demonstrate the ability to cross the BBB (Figure 7). After 3 h, only ~5% of the non-targeted $NaGdF_4$:Yb50% nanoparticles crossed the BBB , whereas ~17% of the targeted $NaGdF_4$:Yb50%-FA crossed. The rate of cell uptake was very gradual for the non-targeted $NaGdF_4$:Yb50% nanoparticles, and only ~14% were able to cross at 24 h. The targeted $NaGdF_4$:Yb50%-FA nanoparticles saturated uptake at 24 h, and ~34% of the nanoparticles were able to cross BBB at 24 h. Both the non-targeted and targeted nanoparticle uptake had little uptake between 24 and 72 h.

Discussion

$NaREF_4$ (RE = rare earth) nanoparticles are known to exist in two phases, the metastable cubic α-phase and the thermodynamically stable hexagonal β-phase.[42] This difference in stability has been exploited

in the focusing of particle size distribution, wherein the more soluble α-phase nanoparticles serve as sacrificial precursors to form the thermodynamically preferred β-phase with narrow distribution.[43–45] This method typically results in larger nanoparticles, although Haase et al has successfully synthesized 5.6 nm β-$NaYF_4$:Yb 20%, Er 2% nanoparticles by heating 10 nm sacrificial α-$NaYF_4$:Yb 20%, Er 2%. [45] It is however a more practical and user-friendly approach to have a single-step method that will allow precise control of size, uniformity and crystal phase.

To form uniform ultrasmall size nanoparticles utilizing a single-step method, it is critical that enough nuclei are formed to ensure uniformity, and the reaction temperature (e.g. 270 °C) is reduced to decrease the particle size.[34, 46, 47] It is well established that hexagonal β-phase $NaGdF_4$ nanoparticles readily form at reaction temperatures below 300 °C.[34, 46] This is due to the large radius of the light lanthanide Gd^{3+} ion that is more polarizable and susceptible to the electron cloud distortion required for the cubic-to-hexagonal phase transformation.[48–50] However, incorporation of the smaller Yb^{3+} ions into the $NaGdF_4$ nanoparticles resulted in an increased free-energy barrier with regards to the formation of the hexagonal phase nanoparticles. Thus, significant doping of the heavier lanthanide Yb^{3+} ion into the host lattice favors the formation of the cubic phase nanoparticles, which are easily produced due to the high surface energy of the ultrasmall nanoparticles. This is in agreement with the results of our synthesis of pure $NaGdF_4$, pure $NaYbF_4$, and $NaGdF_4$:Yb50% nanoparticles (Figure S1). Forming the nuclei at room temperature for 30 minutes and subsequently growing the nanoparticles at 260 °C for 10 minutes yielded hexagonal $NaGdF_4$, while both pure $NaYbF_4$ and $NaGdF_4$:Yb50% resulted in cubic phase nanoparticles as evidenced by their respective XRD patterns (Figure S1). One way to achieve hexagonal β-$NaGdF_4$:Yb50% is to increase the temperature to 300 °C, but this also leads to formation of larger nanoparticles (~ 12 nm).[48] Hence, in order to form hexagonal $NaGdF_4$:Yb50%, the nuclei were allowed to form for 24 h to facilitate the formation of thermodynamically stable, hexagonal nanocrystals, while still maintaining the nanoparticle growth reaction temperature at 260 °C for 10 minutes to tune the size of the nanoparticles. Pure $NaYbF_4$ was also synthesized with 24 h nucleation to check if β-$NaYbF_4$ can form under such conditions. The XRD pattern (Figure S2) revealed a pure cubic α-phase, indicating that the reaction conditions were not enough to transform to hexagonal $NaYbF_4$. Cubic nanoparticle formation was expected since the formulation does not contain Gd^{3+} ions, which have been established to lower the energy barrier for phase transformation of $NaYbF_4$. [48]

To render the β-$NaGdF_4$:Yb50% nanoparticles useful for biological applications, it is necessary to modify the hydrophobic oleic-capped surface with a biocompatible, hydrophilic ligand. The proximity of water protons to the surface of the nanoparticles is critical in achieving high T1 relaxivity, which can be controlled through a surface coating strategy.[51] Phase transfer via ligand exchange was then performed to ensure efficient surface hydration. Removal of oleic acid avoids the formation of long hydrophobic chains that could render the Gd on the surface of the nanoparticles inaccessible to water. [52] In this case, cysteine-DTPA replaced oleic acid on the surface of the nanoparticles to form a stable

monodisperse aqueous suspension. The small increase in the hydrodynamic diameter post-surface modification indicates the formation of a compact hydrophilic surface.

The potential toxicity of the non-targeted nanoparticles was investigated to assess their practical usability in a biological environment. One major challenge in the development of a Gd-based contrast agent is the inherent toxicity of the Gd^{3+} ion when dissociated from its chelate *in vivo*.[53] In the nanocrystal form (i.e., $NaGdF_4$), the hexagonal phase provides a stable matrix that eliminates transmetallation with endogenous metal ions (i.e., Cu^{2+}, Zn^{2+}, Fe^{2+}/Fe^{3+}) [54–57] and hinders any leaching of toxic free Gd^{3+} ions. [58, 59] The very low concentration of Gd^{3+} when dialyzed against H_2O demonstrates the high stability of the nanoparticles against dissolution attributed to their thermodynamically stable hexagonal phase. [60] However, the presence of elevated phosphate levels resulted in a significant increase in leakage, although still a low percentage of Gd^{3+} indicating the stability of the nanoparticles in the physiological environment.

It has been demonstrated that the capping ligand has stabilizing effects and can sequester the free Gd^{3+} ions through chelation.[47, 61, 62] To further investigate and minimize the Gd^{3+} leakage, two strategies could be pursued to improve the design of the surface ligand in relation to the Gd^{3+} release. First, the amount of DTPA conjugated to cysteine could be optimized. Second, DTPA can be replaced with other polyaminocarboxylate ligands such as 1,4,7,10-tetraazacyclododecane-1,4,7,10-tetraacetic acid (DOTA) and derivatives, which are known to form lanthanide complexes with high kinetic stability.[63, 64]

No intrinsic cytotoxicity from the nanoparticles was observed at a concentration as high as 125 µg/mL, even at prolonged exposure time (i.e., 48 h). In vivo clearance study show that the nanoparticles are cleared from the body within days (i.e., 4 days). Furthermore, the fact that the nanoparticles can be cleared through hepatobiliary excretion indicates a decrease in kidney load compared to commercially available Gd^{3+} chelates for MRI (i.e., Gd-DTPA) [8] which are primarily cleared renally. This can potentially avoid contrast-induced nephropathy, a form of acute renal failure caused by exposure to the contrast media, and may lower the risk for developing nephrogenic systemic fibrosis triggered in patients with advanced kidney disease.[65]

After establishing the biocompatibility of the nanoparticles, their ability to be used for dual MR/CT imaging was verified. *In vitro* experiments revealed a substantially higher T1-relaxivity of the nanoparticles compared to a commercial Gd^{3+} chelate at both room temperature and at physiological temperature (37 °C) (Fig. 4a), which may be attributed to the slower tumbling rate of the nanoparticle than the chelate. [66] The higher T1 relaxivity values exhibited by the ultrasmall $NaGdF_4$:Yb50% nanoparticles compared to clinically-utilized Gd-DTPA, and their low r_2/r_1 ratio value falling below 2 (1.47 at T = 25 °C and 1.31 T = 37 °C calculated from Figure S5) demonstrate their potential to serve as an effective T1 MR imaging contrast agent. [67] In addition, the high atomic number of Yb induced enhanced CT signal comparable with iohexol. These results confirm the promise of these nanoparticles in MR/CT multimodal imaging.

The radiosensitization effect of the ultrasmall $NaGdF_4$:Yb50% nanoparticles was then assessed in rat C6 glioma cell line. The survival and the reproductive integrity of the irradiated cells with and without nanoparticle treatment were evaluated through colony formation. One strategy to target the delivery of nanoparticles is to exploit the overexpressed folate receptor, found in many cancer cell lines. C6 cells internalize folic acid-conjugated particles through caveolae-mediated endocytosis.[68] Taking advantage of the highly expressed folate-receptors on C6 glioma cells, nanoparticles with conjugated folic acid ($NaGdF_4$:Yb50%-FA) were prepared to improve cellular uptake.

Results show radiosensitization from both the non-targeted and the targeted nanoparticles. These are in agreement with the recent study investigating the cytotoxicity and radiosensitization of several rare-earth oxide nanoparticles (i.e. Ce, Nd, Gd, La), wherein Gd_2O_3 nanoparticles have shown significant radiosensitization and have generated additional ROS in U-87 MG cell line upon irradiation, without intrinsic toxicity.[69] As evidenced by a significant difference in the surviving colonies between the non-targeted ($NaGdF_4$:Yb50%) and the targeted ($NaGdF_4$:Yb50%-FA) nanoparticles at the same concentration, it is imperative that the nanoparticles be associated with the cells to induce effective damage. A new study has shown near complete destruction of tumor spheroids of human ovarian cancer (OVCAR8) when incubated with gadolinium loaded mesoporous silica nanoparticles (Gd-MSN) prior to exposure to monochromatic 50.25 KeV X-rays. [70] It is worth noting that the Gd-MSNs accumulated in the lysosomes located close to the cell nucleus. This highlights the importance not only of the energy compatibility made possible by using tunable monochromatic beam radiation, but also by the proximity of the radiosensitizers to the nucleus in order to destroy the DNA of the tumor cells. This is due to the low energy and consequent short-range characteristics of the Auger electrons from the Gd^{3+} and Yb^{3+} ions in the nanoparticles provide for the possibility of a highly targeted radiation therapy.

In several reported studies, folate-conjugated drug delivery systems have shown significant nuclear uptake.[71–73] Folic-acid modified silica nanoparticles (FAMSNs) with 100 nm diameter have been observed to accumulate in both the nuclei and the cytoplasm, while unmodified MSNs were found only in the cytoplasm, which confirmed the role of folic acid receptors in the nuclear uptake.[72] Presence of folic acid receptor α (FRα) in the nuclear membrane has been reported. [74, 75] It has also been demonstrated that in the presence of folic acid, FRα translocates to the nucleus. [74, 76] This mechanism of folic acid is highly compatible in the targeted delivery of radiosensitizers. Combined with the additional multi-modal imaging capabilities of the nanoparticles, localization in the tumor can be ensured prior to irradiation, therefore the damage to the surrounding normal cells is minimized if not completely prevented. Furthermore, in vitro transmigration assay confirms that both non-targeted and targeted nanoparticle were able to cross the BBB, with the folic acid-modified nanoparticles being 2.4-fold higher. These results further confirm the effectiveness of using folic acid as target molecule to facilitate transport through BBB.

Conclusions

A novel, ultrasmall sub-5 nm $NaGdF_4$:Yb50% formulation designed to combine imaging and therapy was successfully synthesized and surface modified to render biocompatibility and enhanced cellular uptake. Co-doping of Gd and Yb in equimolar amount allowed the formation of the hexagonal phase of the nanoparticle as well as imparting the nanoparticle with mutifunctionality to be used as a bimodal probe for both MR and CT imaging with excellent T1 contrast for MRI and Hounsfield unit (HU) for CT imaging. Bioconjugation of folic acid to the surface of these nanoparticles facilitated BBB crossing and increased cellular uptake to enable the radiosensitization effects from the emitted low energy Auger electrons in brain cancer cells. *In vitro* radiosensitization experiments in rat C6 glioma cells showed the FA-targeted nanoparticles as very promising radiosensitizers. Hence, these ultrasmall nanoparticles should be further developed to serve as a promising theranostic platform for image-guided radiotherapy.

Materials And Methods

Materials

Gadolinium chloride hexahydrate (99.999%), ytterbium chloride hexahydrate (99.9%), ammonium fluoride (99.99), sodium hydroxide (97%), oleic acid (90%), 1-octadecene (90%), oleylamine (70%), L-cysteine (97%), diethylenetriaminepentaacetic dianhydride (98%), and H_2O_2 (30%) were purchased from Sigma-Aldrich. Methanol (ACS reagent grade, ≥99.8%), hexane (ACS reagent grade, ≥98.5%), and chloroform (ACS reagent grade, ≥99.8%) were purchased from Fisher Scientific. Gadolinium and ytterbium standards for ICP is from Inorganic Ventures and high purity nitric acid for quantitative trace metal analysis at the ppb level is from BDH Aristar® Plus. All materials were used as received.

Synthesis

Synthesis of Ultrasmall α-$NaGdF_4$:Yb50%. Ultrasmall nanoparticles were synthesized by modification of a previously reported procedure.[34, 77] To a 100mL three-neck flask containing 0.5 mmol of $GdCl_3 \times 6H_2O$ and 0.5 mmol of $YbCl_3 \times 6H_2O$ was added 9 mL of oleic acid and 15 mL octadecene. The mixture was heated to 160°C and maintained for 1h under argon gas with constant stirring and then cooled to room temperature. Solution of methanol (10 mL) containing 4 mmol NH_4F and 2.5 mmol NaOH was added and the mixture was stirred for 30 minutes. Temperature is then increased to 100°C and maintained for 30 minutes to remove methanol. The solution was then heated at 260°C for 10min before cooling to room temperature. The nanoparticles were collected by adding excess amount of ethanol and centrifuged at 7000 rcf for 5 min. The precipitate was washed with ethanol and finally dispersed in 10 mL hexane for further uses.

Synthesis of Ultrasmall β-$NaGdF_4$:Yb50%. Ultrasmall nanoparticles were synthesized following the procedure described for α-$NaGdF_4$:Yb50%, except the solution was stirred for 24 h after the addition of methanol solution (10 mL) containing NH_4F (4 mmol) and NaOH (2.5 mmol).

Synthesis of Ultrasmall β-NaGdF$_4$. Ultrasmall nanoparticles were synthesized following the procedure described for α-NaGdF$_4$:Yb50%, except 1.0 mmol of GdCl$_3$ × 6H$_2$O was used.

Synthesis of Ultrasmall α-NaYbF$_4$. Following the procedure described for both *α*-NaGdF$_4$:Yb50% and *β*-NaGdF$_4$:Yb50%, except using 1.0 mmol of YbCl$_3$ × 6H$_2$O, resulted to cubic ultrasmall nanoparticles only.

Ligand Exchange Surface Modification. L-Cysteine (60 mg) and diethylenetriaminepentaacetic (DTPA) dianhydride (20 mg) were dissolved in 30 mL H$_2$O at pH 9 in a 100 mL round bottom flask. To this aqueous solution was added 10 mL chloroform solution containing 10 mg of the oleic-capped ultrasmall nanoparticles. The biphasic mixture was stirred vigorously overnight at room temperature to facilitate the transfer of the nanoparticle to the water phase. Excess ligand was removed by twice centrifugation using Vivaspin-20 centrifugal filters (10kDa MWCO) at 3000 rcf for 15 minutes and the collected nanoparticles were redispersed in water and filtered through a 0.2 μm syringe filter.

Folic-acid Functionalized Ultrasmall Nanoparticles (FA-NaGdF$_4$:Yb50%). Five hundred microliters of folic acid dissolved in DMSO (25 mg/mL) in the presence of triethylamine (6.25 μL) was incubated with 6.5 mg of NHS and 6.25 mg of DCC in the dark overnight and then passed through a 0.2 μm filter. The resulting NHS-activated folic acid was then covalently linked to the amino surface of the nanoparticles provided by cysteine ligand by incubating overnight. The resulting NaGdF$_4$:Yb50%-FA was centrifuged at 16000 rcf for 15minutes, washed twice and stored in 1 mL H$_2$O for future use.

Characterization

The size and the morphology of the resulting nanoparticles were characterized by transmission electron microscopy (TEM) using a JEM-2010 microscope at an acceleration voltage of 200 kV. The hydrodynamic size was determined using Malvern Zetasizer NanoZS90. Powder X-ray diffraction (XRD) patterns were recorded by a RigakuUltima IV diffractometer, using Cu Kα radiation (λ = 0.15418 nm). The 2θ angle of the XRD spectra was recorded at a scanning rate of 1°/min. Inductively coupled plasma-optical emission spectrometer (ICP-OES) analysis was performed using a Thermo Scientific iCAP 6000 instrument. CT tests were performed on microCTInveon model scanner (Siemens Medical Solutions USA, Inc.). T1 and T2 rates of the nanoparticles were measured on a 4.7T preclinical MR scanner using increasing concentrations at both 25°C and 37°C with an inversion-recovery, balanced steady-state free precession (IR-bSSFP) sequence, and a multiecho CPMG scan, respectively, as described elsewhere. [78] T1 and T2 relaxivities ($mM^{-1} \cdot s^{-1}$) of the nanoparticles were compared to the commercially-available Gd-DTPA contrast agent, Magnevist®.

Elemental analysis using ICP-OES

Acid digestion was performed by dissolving 0.15 mg of the nanoparticles in 0.5 mL concentrated high purity HNO$_3$ acid overnight and diluting with a 2% HNO$_3$ solution to a total volume of 15 mL. The single element standards were prepared with the same acid solution.

Gd^{3+} ion leaching

The nanoparticles (5 mL, 1 mM Gd) were loaded into a dialysis tubing (Spectrum, 3.5 kD cut-off) and incubated in H_2O, or DMEM with 10% fetal bovine serum (FBS), or DMEM with 10% FBS supplemented with 10mM phosphate, at 37ºC under sink conditions, with rocking for 3 days. The amount of released Gd^{3+} ions in each solution was measured using ICP-OES.

Biodistribution and Clearance

Animal experiments were performed in compliance with guidelines set by the University at Buffalo Institutional Animal Care and Use Committee. Female CD-1 mice were injected intravenously via tail vein with the nanoparticles in 5% dextrose in water at a dose of 2 mg/kg and housed in metabolic cages for 4 days with free access to water and a standard laboratory diet. Urine and feces were collected separately every 4 h and the mice were sacrificed after 96 h through cervical dislocation. Feces and organs including liver, spleen, kidney, brain, heart and lungs were harvested, frozen and weighed prior to digestion. The urine, feces, and isolated organs were individually placed in a screw cap polypropylene sample tube and to each were added 3 mL of concentrated nitric acid and 2 mL peroxide (30% by weight) and pre-digested for 24 h. The tubes were then placed in a sonicated water bath for a total of 8 h until the samples were completely dissolved. After digestion, each sample was diluted to 100 mL with a 2% solution of nitric acid. The samples were then passed through a 0.2 µm filter and the Gd content was quantified with inductively coupled plasma mass spectrometry (ICP-MS) utilizing a Thermo Scientific XSERIES 2 ICPMS Single Quadrupole Mass Spectrometer.

Cytotoxicity Assay

Cell viability was assessed by the PromegaCellTiter 96® AQ_{ueous} One Solution Cell Proliferation (MTS) Assay. C6 cells were seeded into a 96-well flat-bottom microplate (c.a. 10000 cells/well) at 37°C and 5% CO_2 and allowed to attach to the bottom of the microplate overnight. The cells were then treated with different concentrations of $NaGdF_4$:Yb50% nanoparticles for 12, 24, and 48 h. After the treatment, the cellular medium was changed to remove the nanoparticles and cell debris, and the AQ_{ueous} One Solution reagent (20 µl/well) was added to the cells and incubated for 4 h. Finally, the absorbance was measured at 490 nm using a microplate reader (Opsys MR microplate reader) to determine the percentage of viable cells in the culture relative to the control wells without nanoparticle treatment.

Clonogenic Assay

Clonogenic assay was performed by growing C6 cells in 6-well plates to 90% confluence and were treated with 100 µg/mL concentration of the nanoparticles overnight. Afterwards, cells were irradiated with a 2 Gy X-ray dose using the Faxitron® RX-650 X-ray Irradiator at a dose rate of 0.5 Gy/min delivered using 130 kV energy. Plates were then incubated for 4 h at 37 °C in 5% CO_2, and the cells were subsequently harvested and counted. To assess colony formation, cells were then re-plated at 1000 cells/well in 6-well plates and allowed to form colonies consist of 50 cells. Colonies were then gently washed with Hank's

Balanced Salt Solution (Gibco® HBSS) and fixed with ice-cold methanol for 10 minutes, rinsed once again with HBSS and stained with a 0.5% crystal violet solution for another 10 minutes. Plates were then rinsed with H_2O to remove excess stain and were left to dry at room temperature. Images of the plates were then acquired and saved in the tagged image file format (Tiff). Colony area for each plate was then measured using the ColonyArea plugin[79] in ImageJ. Surviving colonies were normalized against control wells without nanoparticle treatment.

In vitro BBB Transmigration Assay

We made and validated a cell-based *in vitro* transwell model of the BBB in our laboratory and used it to examine BBB properties like quantitative permeability and transendothelial migration of nanoparticles. Our 2D *in vitro* BBB model consists of a two-chamber transwell system in a 12 well culture plate with the upper (luminal) compartment separated from the lower (abluminal) by a semipermeable membrane (polyethylene terephthalate, PET) insert on which the Human brain microvascular endothelial cells (BMVECs) were grown to confluency on the upper side , while a confluent layer of normal human astrocytes (NHAs) was grown on the underside. After tight BBB formation was confirmed by the transendothelial electrical resistance (TEER) measurement, the dispersed nanoparticles (100 µg/mL media) were added to the upper chamber (luminal) and incubated at 37°C in 5% CO_2. Media from the lower chamber (abluminal) were collected at 1, 5, 24, 48 and 72 h incubation times and the Gd content was measured using ICP-OES. Percent transmigration was calculated relative to the initial Gd concentration of the media with 100 µg/mL nanoparticles. The TEER was measured again after their crossing of the BBB to make sure that the transmigration was not due to the compromise of BBB.

Abbreviations

MRI
magnetic resonance imaging
CT
computed tomography
RT
radiotherapy
GBM
glioblastoma
BBB
blood-brain barrier
FBS
fetal bovine serum
DMEM
Dulbecco's modified Eagle medium
DTPA
diethylenetriaminepentaacetic

FA
folic acid
MTS
3-(4,5,-Dimethylthiazol-2-yl)-5-(3-carboxymethoxyphenyl)-2-(4-sulfophenyl)-2*H*-tetrazolium

Declarations

Ethics Approval and Consent to Participate

Animal experiments were performed in compliance with guidelines set by the University at Buffalo Institutional Animal Care and Use Committee.

Consent for Publication

Not applicable

Availability of data and materials

All data generated or analyzed during this study are included in this published article (and its additional information on file).

Competing interests

The authors declare that they have no competing interests

Funding

The work at the Institute For Lasers, Photonics and Biophotonics at The University at Buffalo was supported by funds provided by the office of Vice President for Research and Economic Development. This work utilized shared resources at Roswell Park Comprehensive Cancer Center supported the NCI Cancer Center Support Grant P30CA016156. Research reported in this publication was supported by the National Center for Advancing Translational Sciences of the National Institutes of Health under award number UL1TR001412 and the Roswell Park Alliance Foundation. The content is solely the responsibility of the authors and does not necessarily represent the official views of the NIH.

Authors' contributions

All authors listed have made substantial, direct, and intellectual contributions to the work discussed in this publication. JAD, TYO, SM, GC, and PNP designed the study. JAD, SM, AS, HLH, HH, STG, and JAS performed the experiments and analyzed the data. SM, JFL, and AKS provided resources to ensure completion of the project. MS and PNP provided the funding. PNP supervised the study. All authors

discussed the results and contributed to the final manuscript. All authors read and approved the final manuscript.

Acknowledgments

Not applicable

References

1. Chen G, Roy I, Yang C, Prasad PN. Nanochemistry and Nanomedicine for Nanoparticle-based Diagnostics and Therapy. Chem Rev. 2016;116:2826–85.
2. Dasgupta A, Biancacci I, Kiessling F, Lammers T. Imaging-assisted anticancer nanotherapy. Theranostics. 2020;10:956–67.
3. Chen H, Zhang W, Zhu G, Xie J, Chen X. Rethinking cancer nanotheranostics. Nature Reviews Materials. 2017;2:17024.
4. Yang G, Phua SZF, Bindra AK, Zhao Y. Degradability and Clearance of Inorganic Nanoparticles for Biomedical Applications. Adv Mater. 2019;31:1805730.
5. Kermanizadeh A, Powell LG, Stone V. A review of hepatic nanotoxicology – summation of recent findings and considerations for the next generation of study designs. Journal of Toxicology Environmental Health Part B. 2020;23:137–76.
6. Feliu N, Docter D, Heine M, del Pino P, Ashraf S, Kolosnjaj-Tabi J, Macchiarini P, Nielsen P, Alloyeau D, Gazeau F, et al. In vivo degeneration and the fate of inorganic nanoparticles. Chem Soc Rev. 2016;45:2440–57.
7. Longmire M, Choyke PL, Kobayashi H. Clearance Properties of Nano-sized Particles and Molecules as Imaging Agents: Considerations and Caveats. Nanomedicine (London England). 2008;3:703–17.
8. Yu M, Zheng J. Clearance Pathways and Tumor Targeting of Imaging Nanoparticles. ACS Nano. 2015;9:6655–74.
9. Ye L, Yong K-T, Liu L, Roy I, Hu R, Zhu J, Cai H, Law W-C, Liu J, Wang K, et al. A pilot study in non-human primates shows no adverse response to intravenous injection of quantum dots. Nat Nano. 2012;7:453–8.
10. Ballou B, Ernst LA, Andreko S, Harper T, Fitzpatrick JAJ, Waggoner AS, Bruchez MP. Sentinel Lymph Node Imaging Using Quantum Dots in Mouse Tumor Models. Bioconjug Chem. 2007;18:389–96.
11. Du B, Yu M, Zheng J. Transport and interactions of nanoparticles in the kidneys. Nature Reviews Materials. 2018;3:358–74.
12. Xie M, Xu Y, Huang J, Li Y, Wang L, Yang L, Mao H. **Going even smaller**: **Engineering sub-5 nm nanoparticles for improved delivery**, **biocompatibility**, **and functionality**. *WIREs Nanomedicine and Nanobiotechnology*, **n**/**a**:e1644.

13. Choi HS, Liu W, Liu F, Nasr K, Misra P, Bawendi MG, Frangioni JV. Design Considerations for Tumor-Targeted Nanoparticles. Nature nanotechnology. 2010;5:42–7.
14. Retif P, Pinel S, Toussaint M, Frochot C, Chouikrat R. **Nanoparticles for radiation therapy enhancement: the key parameters**. *Theranostics* 2015.
15. **Quantification of the effect of treatment duration on local-regional failure after definitive concurrent chemotherapy and intensity-modulated radiation therapy for squamous cell carcinoma of the head and neck.** *Head & neck* 2013, **35**:684–688.
16. Penninckx S, Heuskin AC, Michiels C, Lucas S. **Gold Nanoparticles as a Potent Radiosensitizer: A Transdisciplinary Approach from Physics to Patient**. *Cancers (Basel)* 2020, 12.
17. Laprise-Pelletier M, Simão T, Fortin M-A. Gold Nanoparticles in Radiotherapy and Recent Progress in Nanobrachytherapy. Advanced Healthcare Materials. 2018;7:1701460.
18. Ngwa W, Kumar R, Sridhar S, Korideck H, Zygmanski P, Cormack RA, Berbeco R, Makrigiorgos GM. Targeted radiotherapy with gold nanoparticles: current status and future perspectives. Nanomedicine (London England). 2014;9:1063–82.
19. Babaei M, Ganjalikhani M. The potential effectiveness of nanoparticles as radio sensitizers for radiotherapy. BioImpacts: BI. 2014;4:15–20.
20. Bonvalot S, Rutkowski PL, Thariat J, Carrère S, Ducassou A, Sunyach MP, Agoston P, Hong A, Mervoyer A, Rastrelli M, et al. NBTXR3, a first-in-class radioenhancer hafnium oxide nanoparticle, plus radiotherapy versus radiotherapy alone in patients with locally advanced soft-tissue sarcoma (Act.In.Sarc): a multicentre, phase 2–3, randomised, controlled trial. Lancet Oncol. 2019;20:1148–59.
21. Deng J, Xu S, Hu W, Xun X, Zheng L, Su M. Tumor targeted, stealthy and degradable bismuth nanoparticles for enhanced X-ray radiation therapy of breast cancer. Biomaterials. 2018;154:24–33.
22. Erika P, Samuel L, Hynd R, Noriko U, Katsumi K, Yoshiya F, Claude Le S, Sandrine L. Platinum nanoparticles: a promising material for future cancer therapy? Nanotechnology. 2010;21:085103.
23. Li Y, Yun K-H, Lee H, Goh S-H, Suh Y-G, Choi Y. Porous platinum nanoparticles as a high-Z and oxygen generating nanozyme for enhanced radiotherapy in vivo. Biomaterials. 2019;197:12–9.
24. Klein S, Sommer A, Distel LVR, Neuhuber W, Kryschi C. Superparamagnetic iron oxide nanoparticles as radiosensitizer via enhanced reactive oxygen species formation. Biochem Biophys Res Commun. 2012;425:393–7.
25. Khoei S, Mahdavi SR, Fakhimikabir H, Shakeri-Zadeh A, Hashemian A. The role of iron oxide nanoparticles in the radiosensitization of human prostate carcinoma cell line DU145 at megavoltage radiation energies. Int J Radiat Biol. 2014;90:351–6.
26. Cassim SM, Giustini AJ, Petryk AA, Strawbridge RA, Hoopes PJ: **Iron Oxide Hyperthermia And Radiation Cancer Treatment**. *Proceedings of SPIE–the International Society for Optical Engineering* 2009, **7181**:718100.
27. Dufort S, Appelboom G, Verry C, Barbier EL, Lux F, Bräuer-Krisch E, Sancey L, Chang SD, Zhang M, Roux S, et al. Ultrasmall theranostic gadolinium-based nanoparticles improve high-grade rat glioma survival. Journal of Clinical Neuroscience. 2019;67:215–9.

28. Le Duc G, Roux S, Paruta-Tuarez A, Dufort S, Brauer E, Marais A, Truillet C, Sancey L, Perriat P, Lux F, Tillement O. Advantages of gadolinium based ultrasmall nanoparticles vs molecular gadolinium chelates for radiotherapy guided by MRI for glioma treatment. Cancer Nanotechnol. 2014;5:4.
29. Verry C, Sancey L, Dufort S, Le Duc G, Mendoza C, Lux F, Grand S, Arnaud J, Quesada JL, Villa J, et al. Treatment of multiple brain metastases using gadolinium nanoparticles and radiotherapy: NANO-RAD, a phase I study protocol. BMJ Open. 2019;9:e023591.
30. Xing H, Bu W, Ren Q, Zheng X, Li M, Zhang S, Qu H, Wang Z, Hua Y, Zhao K, et al. A NaYbF4: Tm3 + nanoprobe for CT and NIR-to-NIR fluorescent bimodal imaging. Biomaterials. 2012;33:5384–93.
31. Xing H, Zheng X, Ren Q, Bu W, Ge W, Xiao Q, Zhang S, Wei C, Qu H, Wang Z, et al: **Computed tomography imaging-guided radiotherapy by targeting upconversion nanocubes with significant imaging and radiosensitization enhancements**. 2013, 3:1751.
32. He M, Huang P, Zhang C, Hu H, Bao C, Gao G, He R, Cui D. Dual Phase-Controlled Synthesis of Uniform Lanthanide-Doped NaGdF4 Upconversion Nanocrystals Via an OA/Ionic Liquid Two-Phase System for In Vivo Dual-Modality Imaging. Adv Func Mater. 2011;21:4470–7.
33. Liu Y, Ai K, Liu J, Yuan Q, He Y, Lu L. A High-Performance Ytterbium-Based Nanoparticulate Contrast Agent for In□Vivo X-Ray Computed Tomography Imaging. Angew Chem Int Ed. 2012;51:1437–42.
34. Johnson NJJ, Oakden W, Stanisz GJ, Scott Prosser R, van Veggel FCJM. Size-Tunable, Ultrasmall NaGdF4 Nanoparticles: Insights into Their T1 MRI Contrast Enhancement. Chem Mater. 2011;23:3714–22.
35. Holland EC. Glioblastoma multiforme: The terminator. Proc Natl Acad Sci USA. 2000;97:6242–4.
36. Afzalipour R, Khoei S, Khoee S, Shirvalilou S, Jamali Raoufi N, Motevalian M, Karimi MR. Dual-Targeting Temozolomide Loaded in Folate-Conjugated Magnetic Triblock Copolymer Nanoparticles to Improve the Therapeutic Efficiency of Rat Brain Gliomas. ACS Biomaterials Science Engineering. 2019;5:6000–11.
37. Wu D, Pardridge WM. Blood-brain barrier transport of reduced folic acid. Pharm Res. 1999;16:415–9.
38. Kong B, Seog JH, Graham LM, Lee SB. Experimental considerations on the cytotoxicity of nanoparticles. Nanomedicine (London England). 2011;6:929–41.
39. Lewinski N, Colvin V, Drezek R. Cytotoxicity of Nanoparticles. Small. 2008;4:26–49.
40. Mahajan SD, Aalinkeel R, Sykes DE, Reynolds JL, Bindukumar B, Adal A, Qi M, Toh J, Xu G, Prasad PN, Schwartz SA. Methamphetamine alters blood brain barrier permeability via the modulation of tight junction expression: Implication for HIV-1 neuropathogenesis in the context of drug abuse. Brain research. 2008;1203:133–48.
41. Singh A, Kim W, Kim Y, Jeong K, Kang CS, Kim Y, Koh J, Mahajan SD, Prasad PN, Kim S. Multifunctional Photonics Nanoparticles for Crossing the Blood–Brain Barrier and Effecting Optically Trackable Brain Theranostics. Adv Func Mater. 2016;26:7057–66.
42. Mai H-X, Zhang Y-W, Si R, Yan Z-G, Sun L-d, You L-P, Yan C-H. High-Quality Sodium Rare-Earth Fluoride Nanocrystals: Controlled Synthesis and Optical Properties. J Am Chem Soc. 2006;128:6426–36.

43. Dühnen S, Rinkel T, Haase M. Size Control of Nearly Monodisperse β-NaGdF4 Particles Prepared from Small α-NaGdF4 Nanocrystals. Chem Mater. 2015;27:4033–9.
44. Naduviledathu Raj A, Rinkel T, Haase M. Ostwald Ripening, Particle Size Focusing, and Decomposition of Sub-10 nm NaREF4 (RE = La, Ce, Pr, Nd) Nanocrystals. Chem Mater. 2014;26:5689–94.
45. Rinkel T, Nordmann J, Raj AN, Haase M. Ostwald-ripening and particle size focussing of sub-10 nm NaYF4 upconversion nanocrystals. Nanoscale. 2014;6:14523–30.
46. Jin X, Fang F, Liu J, Jiang C, Han X, Song Z, Chen J, Sun G, Lei H, Lu L. An ultrasmall and metabolizable PEGylated NaGdF4:Dy nanoprobe for high-performance T1/T2-weighted MR and CT multimodal imaging. Nanoscale. 2015;7:15680–8.
47. Xing H, Zhang S, Bu W, Zheng X, Wang L, Xiao Q, Ni D, Zhang J, Zhou L, Peng W, et al. Ultrasmall NaGdF4 Nanodots for Efficient MR Angiography and Atherosclerotic Plaque Imaging. Adv Mater. 2014;26:3867–72.
48. Damasco JA, Chen G, Shao W, Ågren H, Huang H, Song W, Lovell JF, Prasad PN. Size-Tunable and Monodisperse Tm3+/Gd3+-Doped Hexagonal NaYbF4 Nanoparticles with Engineered Efficient Near Infrared-to-Near Infrared Upconversion for In Vivo Imaging. ACS Appl Mater Interfaces. 2014;6:13884–93.
49. Noculak A, Podhorodecki A, Pawlik G, Banski M, Misiewicz J. Ion-ion interactions in [small beta]-NaGdF4:Yb3+,Er3 + nanocrystals - the effect of ion concentration and their clustering. Nanoscale. 2015;7:13784–92.
50. Wang F, Han Y, Lim C, Lu Y, Wang J, Xu J, Chen H, Zhang C, Hong M, Liu X. Simultaneous phase and size control of upconversion nanocrystals through lanthanide doping. Nature. 2010;463:1061–5.
51. Johnson NJJ, He S, Nguyen Huu VA, Almutairi A. Compact Micellization: A Strategy for Ultrahigh T1 Magnetic Resonance Contrast with Gadolinium-Based Nanocrystals. ACS Nano. 2016;10:8299–307.
52. Fang J, Chandrasekharan P, Liu XL, Yang Y, Lv YB, Yang CT, Ding J. Manipulating the surface coating of ultra-small Gd2O3 nanoparticles for improved T1-weighted MR imaging. Biomaterials. 2014;35:1636–42.
53. Zhou Z, Lu Z-R. Gadolinium-Based Contrast Agents for MR Cancer Imaging. Wiley interdisciplinary reviews Nanomedicine nanobiotechnology. 2013;5:1–18.
54. Morcos SK. Extracellular gadolinium contrast agents: Differences in stability. Eur J Radiol. 2008;66:175–9.
55. Rabiet M, Letouzet M, Hassanzadeh S, Simon S. Transmetallation of Gd-DTPA by Fe3+, Cu2 + and Zn2 + in water: batch experiments and coagulation-flocculation simulations. Chemosphere. 2014;95:639–42.
56. Telgmann L, Wehe CA, Kunnemeyer J, Bulter AC, Sperling M, Karst U. Speciation of Gd-based MRI contrast agents and potential products of transmetalation with iron ions or parenteral iron supplements. Anal Bioanal Chem. 2012;404:2133–41.

57. Wu X, Zong Y, Ye Z, Lu Z-R. Stability and Biodistribution of a Biodegradable Macromolecular MRI Contrast Agent Gd-DTPA Cystamine Copolymers (GDCC) in Rats. Pharm Res. 2010;27:1390–7.
58. Chen G, Ohulchanskyy TY, Law WC, Agren H, Prasad PN. Monodisperse NaYbF4: Tm3+/NaGdF4 core/shell nanocrystals with near-infrared to near-infrared upconversion photoluminescence and magnetic resonance properties. Nanoscale. 2011;3:2003–8.
59. Kumar R, Nyk M, Ohulchanskyy TY, Flask CA, Prasad PN. Combined Optical and MR Bioimaging Using Rare Earth Ion Doped NaYF4 Nanocrystals. Adv Func Mater. 2009;19:853–9.
60. Lisjak D, Plohl O, Ponikvar-Svet M, Majaron B. Dissolution of upconverting fluoride nanoparticles in aqueous suspensions. RSC Advances. 2015;5:27393–7.
61. Ahrén M, Selegård L, Klasson A, Söderlind F, Abrikossova N, Skoglund C, Bengtsson T, Engström M, Käll P-O, Uvdal K. Synthesis and Characterization of PEGylated Gd2O3 Nanoparticles for MRI Contrast Enhancement. Langmuir. 2010;26:5753–62.
62. Mekuria SL, Debele TA, Tsai H-C. Encapsulation of Gadolinium Oxide Nanoparticle (Gd2O3) Contrasting Agents in PAMAM Dendrimer Templates for Enhanced Magnetic Resonance Imaging in Vivo. ACS Appl Mater Interfaces. 2017;9:6782–95.
63. Tei L, Baranyai Z, Gaino L, Forgacs A, Vagner A, Botta M. Thermodynamic stability, kinetic inertness and relaxometric properties of monoamide derivatives of lanthanide(iii) DOTA complexes. Dalton Trans. 2015;44:5467–78.
64. Zhu X, Lever SZ. Formation kinetics and stability studies on the lanthanide complexes of 1,4,7,10-tetraazacyclododecane-N,N',N'',N'''-tetraacetic acid by capillary electrophoresis. Electrophoresis. 2002;23:1348–56.
65. Perazella MA. Current status of gadolinium toxicity in patients with kidney disease. Clin J Am Soc Nephrol. 2009;4:461–9.
66. Hou Y, Qiao R, Fang F, Wang X, Dong C, Liu K, Liu C, Liu Z, Lei H, Wang F, Gao M. NaGdF4 Nanoparticle-Based Molecular Probes for Magnetic Resonance Imaging of Intraperitoneal Tumor Xenografts in Vivo. ACS Nano. 2013;7:330–8.
67. Zhang W, Liu L, Chen H, Hu K, Delahunty I, Gao S, Xie J. Surface impact on nanoparticle-based magnetic resonance imaging contrast agents. Theranostics. 2018;8:2521–48.
68. Dong S, Cho HJ, Lee YW, Roman M. Synthesis and Cellular Uptake of Folic Acid-Conjugated Cellulose Nanocrystals for Cancer Targeting. Biomacromol. 2014;15:1560–7.
69. Lu VM, Crawshay-Williams F, White B, Elliot A, Hill MA, Townley HE. Cytotoxicity, dose-enhancement and radiosensitization of glioblastoma cells with rare earth nanoparticles. Artificial Cells Nanomedicine Biotechnology. 2019;47:132–43.
70. Matsumoto K, Saitoh H, Doan TLH, Shiro A, Nakai K, Komatsu A, Tsujimoto M, Yasuda R, Kawachi T, Tajima T, Tamanoi F. Destruction of tumor mass by gadolinium-loaded nanoparticles irradiated with monochromatic X-rays: Implications for the Auger therapy. Sci Rep. 2019;9:13275.
71. Goren D, Horowitz AT, Tzemach D, Tarshish M, Zalipsky S, Gabizon A: **Nuclear Delivery of Doxorubicin via Folate-targeted Liposomes with Bypass of Multidrug-resistance Efflux Pump**. *Clinical*

Cancer Research 2000, **6**:1949.

72. Porta F, Lamers GEM, Morrhayim J, Chatzopoulou A, Schaaf M, den Dulk H, Backendorf C, Zink JI, Kros A. Folic Acid-Modified Mesoporous Silica Nanoparticles for Cellular and Nuclear Targeted Drug Delivery. Advanced Healthcare Materials. 2013;2:281–6.
73. Wang M, Long J, Zhang S, Liu F, Zhang X, Zhang X, Sun L, Ma L, Yu C, Wei H. Folate-Targeted Anticancer Drug Delivery via a Combination Strategy of a Micelle Complex and Reducible Conjugation. ACS Biomaterials Science Engineering. 2020;6:1565–72.
74. Boshnjaku V, Shim K-W, Tsurubuchi T, Ichi S, Szany EV, Xi G, Mania-Farnell B, McLone DG, Tomita T, Mayanil CS. Nuclear localization of folate receptor alpha: a new role as a transcription factor. Scientific reports. 2012;2:980–0.
75. Bozard BR, Ganapathy PS, Duplantier J, Mysona B, Ha Y, Roon P, Smith R, Goldman ID, Prasad P, Martin PM, et al. Molecular and Biochemical Characterization of Folate Transport Proteins in Retinal Müller Cells. Invest Ophthalmol Vis Sci. 2010;51:3226–35.
76. Mohanty V, Siddiqui MR, Tomita T, Mayanil CS. Folate receptor alpha is more than just a folate transporter. Neurogenesis. 2017;4:e1263717.
77. Li Z, Zhang Y. An efficient and user-friendly method for the synthesis of hexagonal-phase NaYF(4):Yb, Er/Tm nanocrystals with controllable shape and upconversion fluorescence. Nanotechnology. 2008;19:345606.
78. Dorazio SJ, Tsitovich PB, Siters KE, Spernyak JA, Morrow JR. Iron(II) PARACEST MRI Contrast Agents. J Am Chem Soc. 2011;133:14154–6.
79. Guzmán C, Bagga M, Kaur A, Westermarck J, Abankwa D. ColonyArea: An ImageJ Plugin to Automatically Quantify Colony Formation in Clonogenic Assays. PLOS ONE. 2014;9:e92444.

Figures

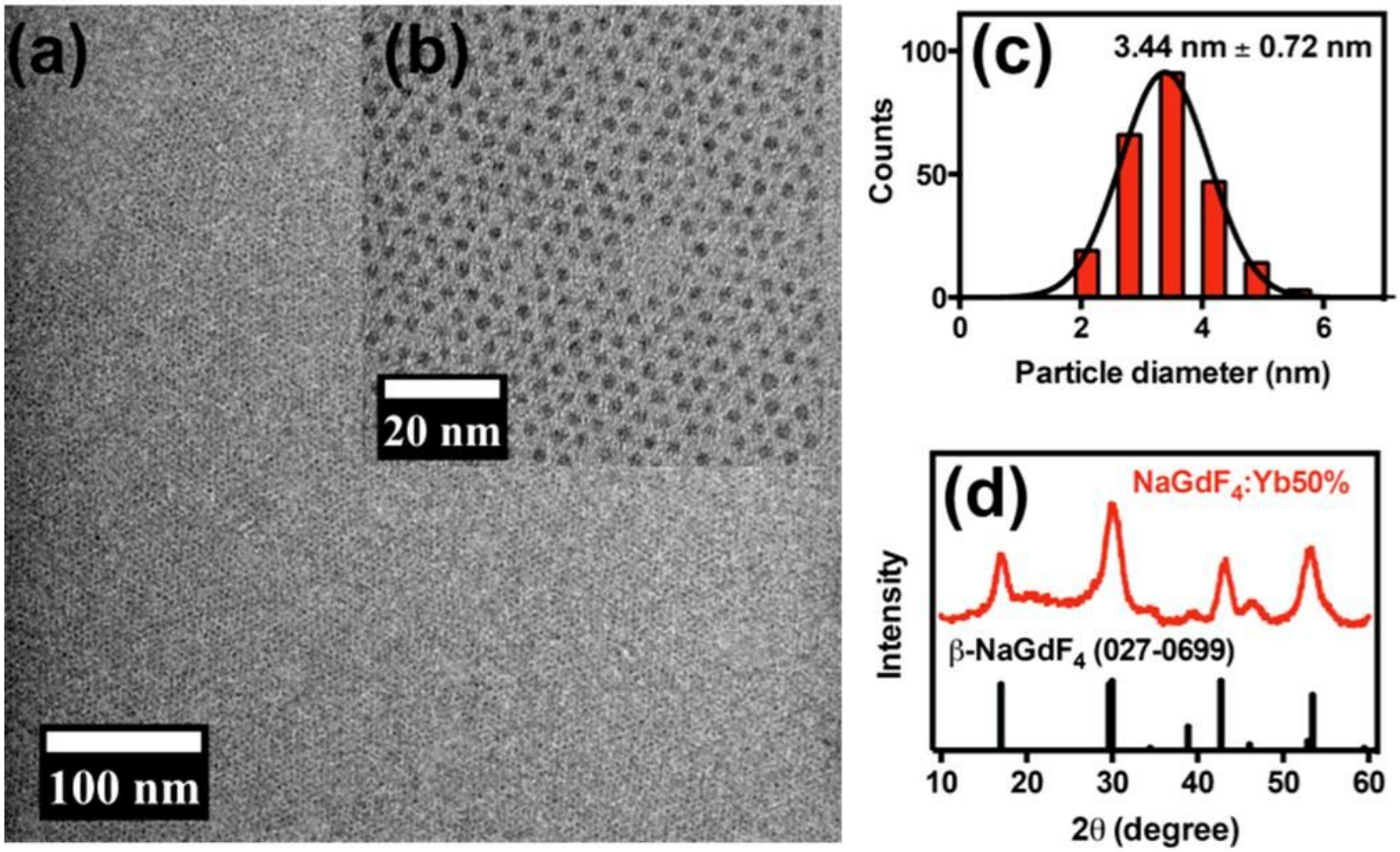

Figure 1

Characterization of β-NaGdF4:Yb50%. (a) TEM and (b) HRTEM images show the synthesized nanoparticles are uniform and monodisperse with core diameter less than 5nm as indicated in the (c) size distribution determined from several TEM images. (d)XRD reveals the hexagonal crystal structure, which is the thermodynamically stable phase of the nanocrystal.

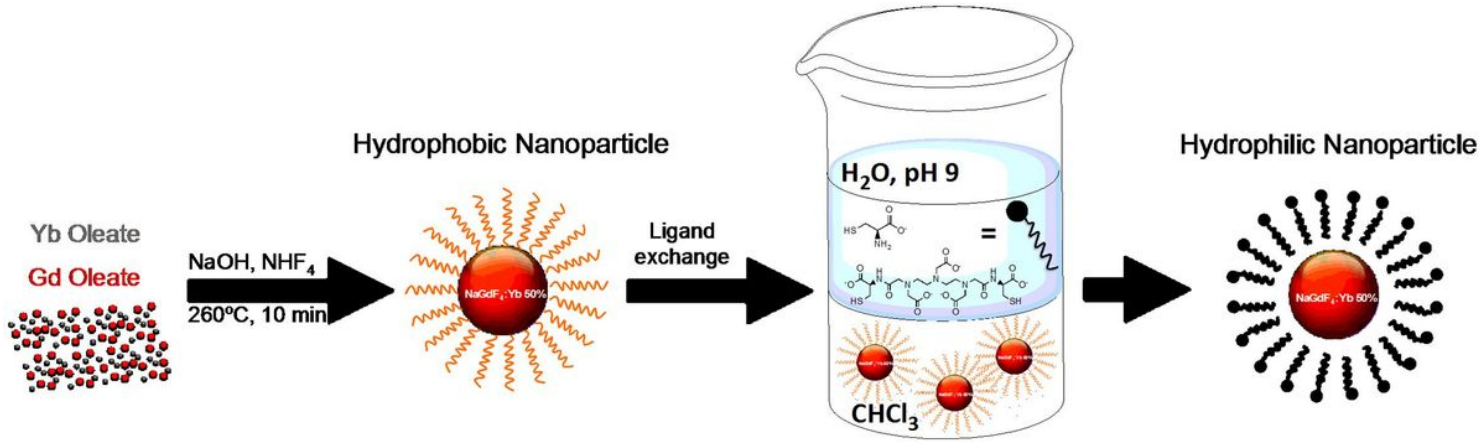

Figure 2

Schematic illustration of the synthesis and surface modification of ultrasmall oleic acid-stabilized NaGdF4:Yb50% nanoparticles.

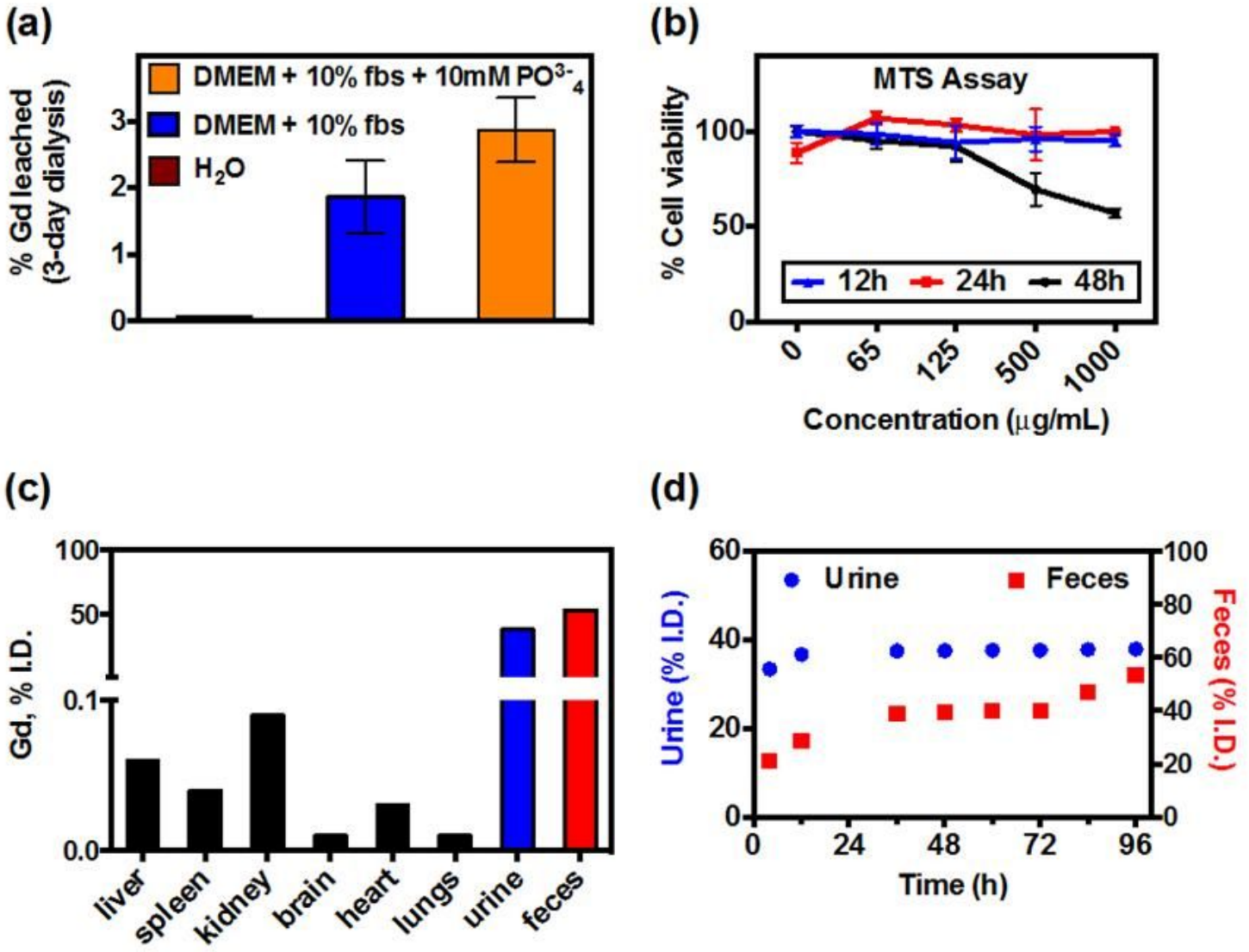

Figure 3

Biocompatibilty of H2O-dispersed β-NaGdF4:Yb50% (a) ICP-OES analysis of the Gd3+ ions leaching from the nanoparticles after 3 days of dialysis. (b) Cell viability when incubated with the nanoparticles evaluated by MTS assay. (c) Biodistribution at 4 h post-injection via tail vein measured by ICP-MS. (d) Cumulative renal and fecal clearance of the nanoparticles monitored by Gd3+ determination via ICP-MS.

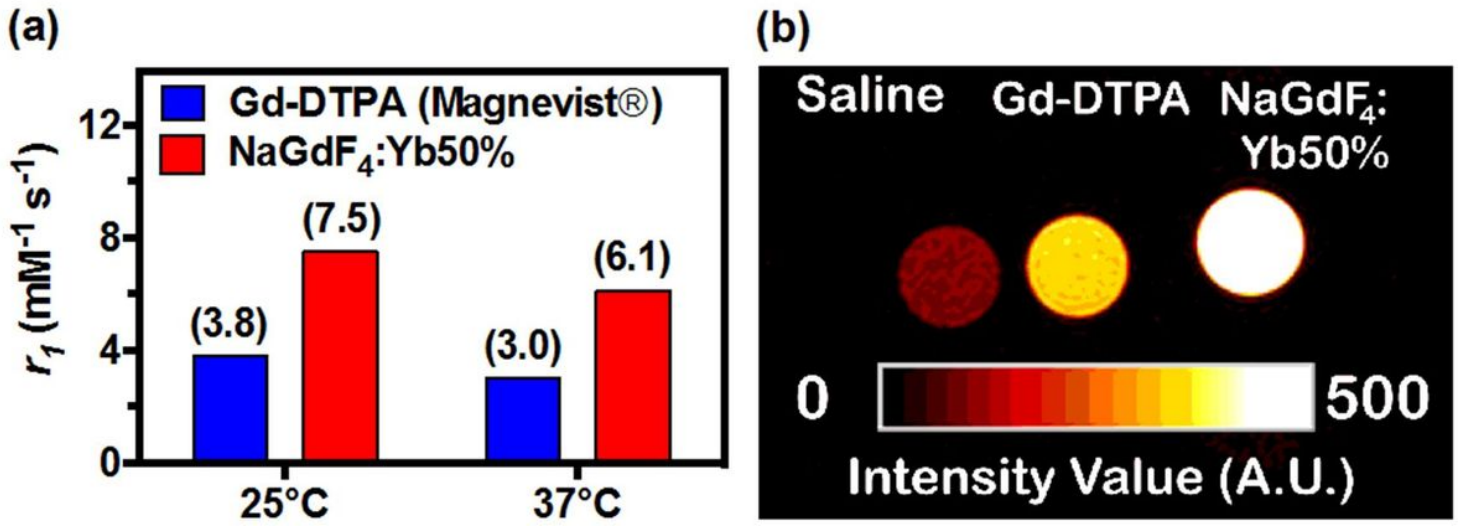

Figure 4

(a) Comparison of in vitro, longitudinal relaxivity values (r1), at 4.7T for commercially-available Gd-DTPA vs ultrasmall NaGdF4:Yb50% at 25°C and 37°C. (b) Pseudo-colored, T1-weighted MR image for saline, Gd-DTPA and ultrasmall NaGdF4:Yb50%. Ultrasmall nanoparticles and Gd-DTPA samples contain the same concentration of Gd3+ (200μM).

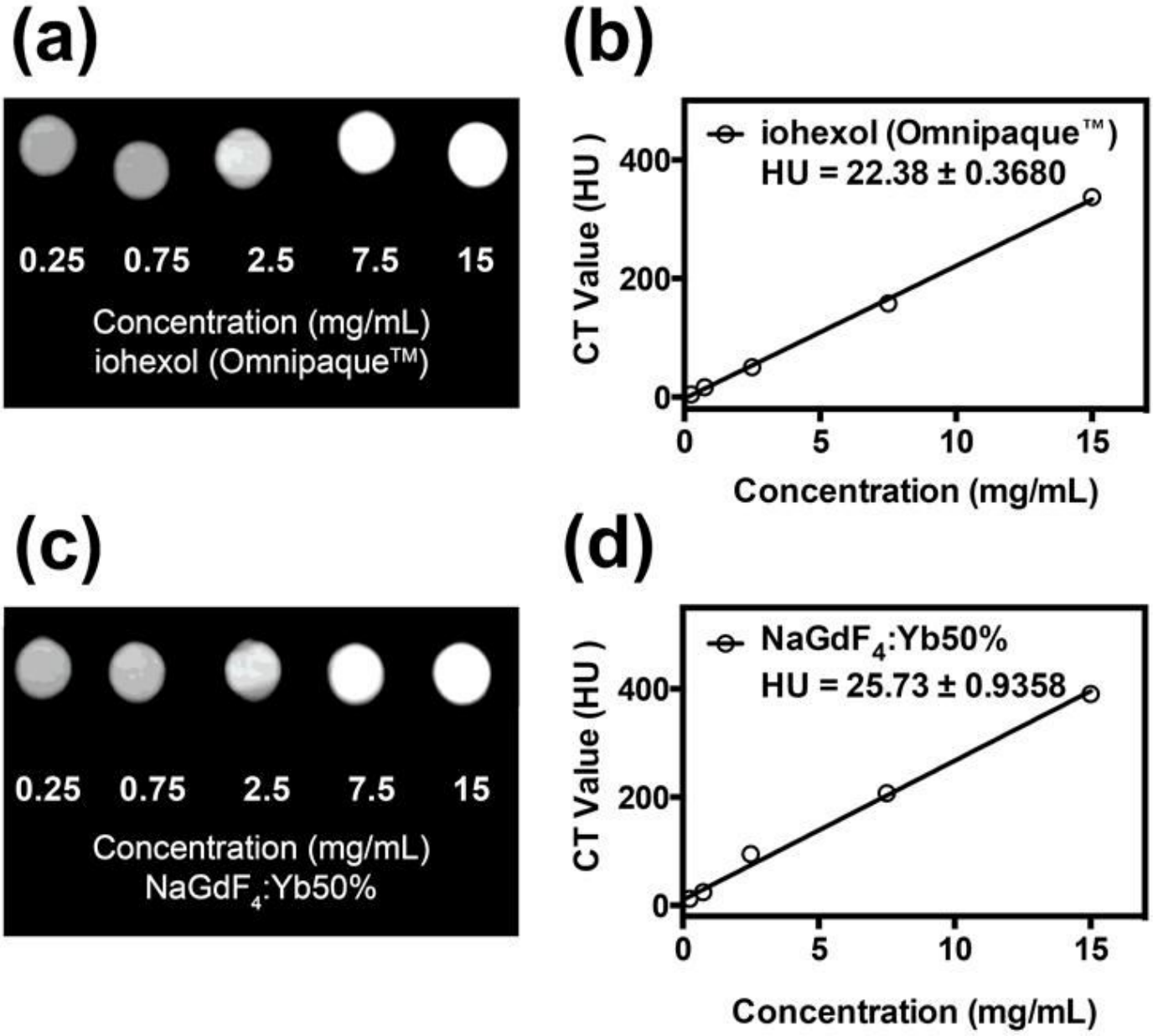

Figure 5

(a) and (c) CT images and the respective (b) and (d) HU measurements of iohexol and NaGdF4:Yb50% nanoparticles at different concentrations in H2O.

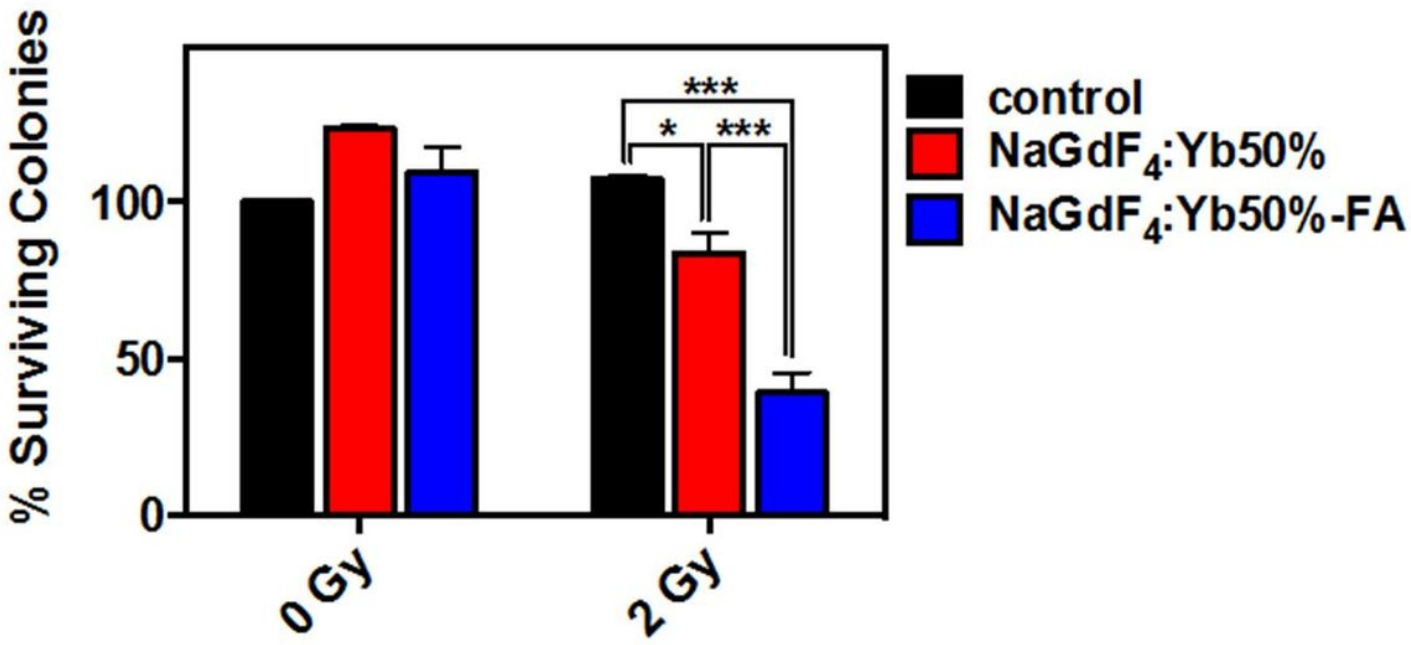

Figure 6

Effect of the nanoparticle treatment on the colony formation of C6 cells following 2 Gy X-ray irradiation. The cells were incubated with the nanoparticles overnight prior to the irradiation. The surviving fraction for each treatment was tested using two-way ANOVA with Tukey's multiple comparisons test. (*P<0.05; *** P<0.001)

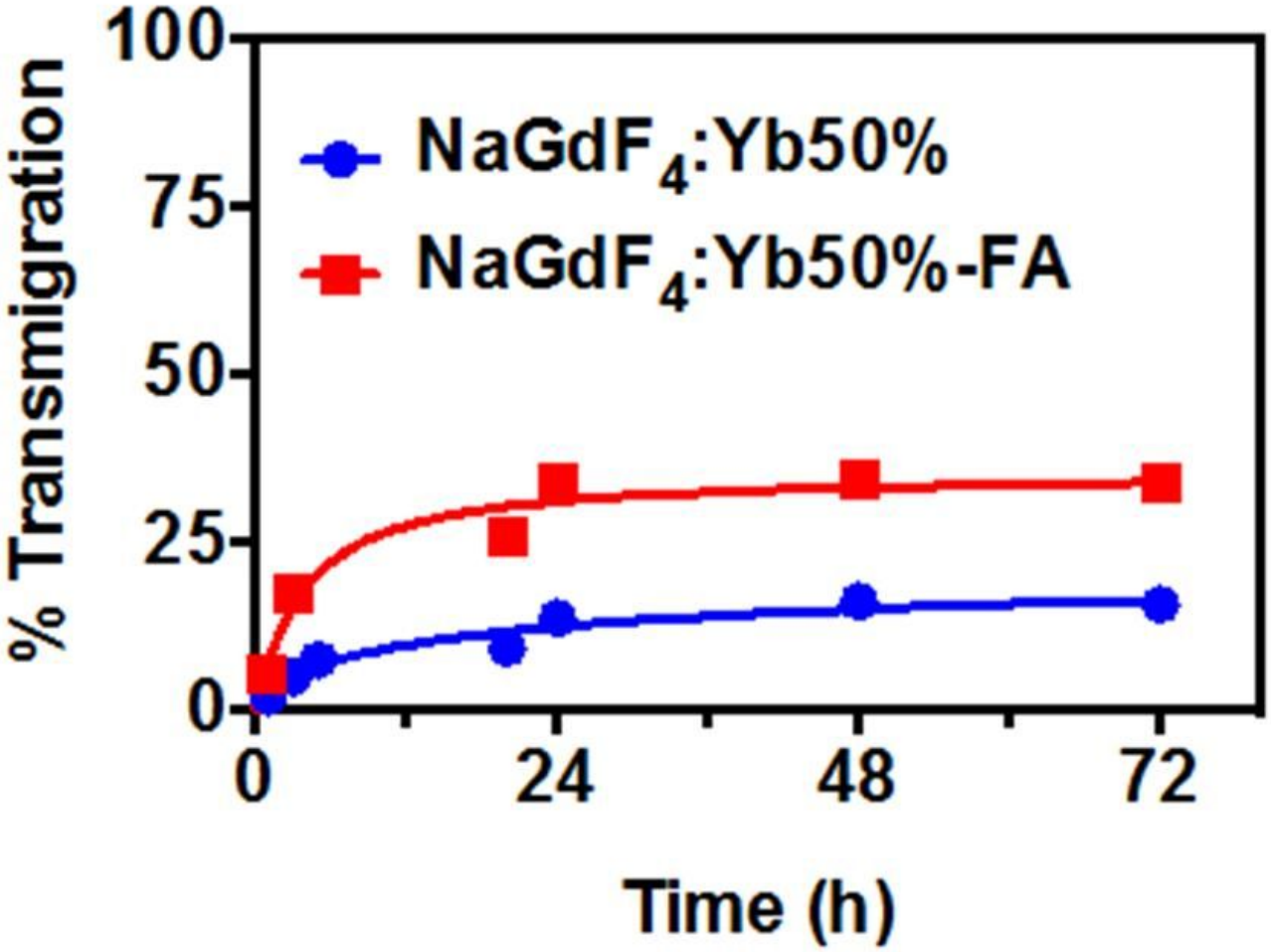

Figure 7

Transmigration of nanoparticles across the in vitro BBB.

Supplementary Files

This is a list of supplementary files associated with this preprint. Click to download.

- SupplementaryInformationCancerNanotech.docx